ADVANCED THERMAL AND SOLAR RADIATION PRESSURE MODELLING FOR HIGH-AREA-TO-MASS RATIO (HAMR) OBJECTS: YORP UND YARKOWSKI

C. Frueh[(1)]

[(1)]*Assistant Professor, Assistant Professor, School of Aeronautics and Astronautics Purdue University, 701 W. Stadium Ave., West Lafayette, IN 47907-2045, 765-494-7436, cfrueh@purdue.edu*

Abstract: *Commonly used models for the thermal re-radiation of space objects are mathematically very simple but also insufficient. The radiation transport through the objects is either neglected or semi-empirically fitted with so-called lag parameters. The simplified models without lag parameters assume no thermal radiation if the two sides of the object have identical thermal radiation parameters and temperature drops to zero immediately when shadow is reached. This is not realistic and leads to a wrong determination of the effects of thermal radiation, so-called YORP and YARKOWSKI effects on the orbit and attitude of uncontrolled objects. This paper suggests an improved thermal model, which is still computationally inexpensive.*

Keywords: *space debris, astrodynamics, SRP modeling, shadow effects*

1. Introduction

In 2004, T. Schildknecht [1, 2] discovered a new class of objects with surprisingly high area-to-mass ratios. This class of objects is highly perturbed by non-gravitational accelerations, especially solar radiation pressure for those objects, which are in near geostationary orbits. Direct solar radiation pressure is one force acting on the object via reflection and absorption forces, that alter both, the attitude of the object and have effects on the orbit. Significant effort has been spent in the prediction of high area-to-mass ratio objects, which are solar radiation pressure perturbed and to model correctly the coupled orbit-attitude motion of non-spherical objects [3, 4, 5, 6, 7].

The effects of direct radiation pressure has not only be investigated in the space debris physics, but is mainly known for the orbit and attitude modeling of asteroids. In 1851 Öpik [8] recalled a pamphlet from Yarkovski, in which the effect of anisotropic thermal re-radiation was discussed, being an additional force acting on a celestial body and depending on the area-to-mass ratio of the asteroid may significantly alter its orbital evolution. Starting in 1954, O'Keefe, Radzievskii and Paddack realized that the effect is not only significant on the orbital evolution but also on the attitude of the object, which can result in significant rotation of a body. This gave rise to the name YORP effect [9].

To a very limited extend YORP effects have been studied for space debris objects [10]. In that work, emphasis has been laid on the long term effects and if YORP could be an explanation of rotation rates of large bodies such as upper stages and complete decommissioned satellites. This current work has a different purpose. It focuses on the high area-to-mass ratio objects (HAMR) and discerns if in the short term prediction between two observation periods, YORP and Yarkosvski effect have a significant influence on both the attitude and the orbit of the object, such that they should necessarily be modeled in order to have a reliable prediction that allows re-detection of those objects. The

mathematical theory of modeling reflection and thermal radiation effects is shown and two cases are simulated, a flat object with non-uniform reflection properties and a folded object, which is significantly affected by self-shadowing. Both types of objects are known to spin up rapidly within shortest time periods due to reflection forces alone. Their orbits are significantly altered by their attitude motion [3, 5]. Initial studies on this subject have been performed by the author [11], for sake of completeness the findings are fully included here.

2. Orbit and Attitude Dynamics

The fully coupled orbit-attitude motion without thermal re-radiation has been already investigated and explained in greater detail [3].The geocentric equations of motion for an object are described as follows:

$$\ddot{\vec{x}} \quad = -GM\nabla V(\vec{x}) - G\sum_{k=1,2} M_k \left[\frac{\vec{x}-\vec{x}_k}{|\vec{x}-\vec{x}_k|^3} + \frac{\vec{x}_k}{x_k^3}\right] + \sum_l \vec{a}_l \tag{1}$$

where $\vec{x}$ is the geocentric position of the object, G the gravitational constant, M the Earth mass and $V(\vec{x})$ the Earth gravitational potential. For its representation the formulation of Pines [12] was chosen, and transformed in the Earth centered space fixed coordinate system. The third body gravitational perturbations of the Sun and Moon (k=1,2) with the states $\vec{x}_k$ have also been taken into account. Finally, $\sum \vec{a}$ is the sum over all non-gravitational accelerations acting on the satellite. These latter perturbations can include accelerations due to direct solar radiation pressure (SRP) and, hence, the attitude dependence finds its way into the equations of motion. If attitude dynamics are modeled, these must be included in the integration of the equations of motion.

The dynamic equations of motion a rigid body can be calculated using Euler's equations [13], where the body is approximated as sum over the n facet- and volume elements approximating the body's shape and mass, respectively:

$$\frac{d}{dt}(I\vec{\omega}) = \sum_{l=1}^{m} \vec{\tau}_l - \vec{\omega}\times(I\vec{\omega}) \quad \text{where:} \quad I_{\alpha\beta} = \sum_{k=1}^{n} m_k(r_k^2\delta_{\alpha\beta} - z_{k,\alpha}z_{k,\beta}), r_k = \sqrt{\sum_{\alpha,\beta,\gamma} z_k^2}$$

where $\vec{\omega}(t)$ is the angular velocity body rate. $I_{\alpha\beta}$ is the tensors of the net moments of inertia of each volume element, with mass m_k located at position $z_{\alpha\beta\gamma}$, δ is the kronecker delta. The moments of inertia are constant over time, under the assumption of a rigid body. $\sum_l \vec{\tau}_l$ represents the sum of the disturbance torques. In the case of space debris objects no control torques are present. The vectors are represented and time-derivatives taken in a body-fixed reference frame. The kinematic equations can be represented in terms of attitude as quaternions [13]:

$$\frac{d\vec{q}}{dt} = 0.5\cdot\Omega\cdot\vec{q} \qquad \text{with:} \quad \Omega = \begin{bmatrix} 0 & \omega_3 & -\omega_2 & \omega_1 \\ -\omega_3 & 0 & \omega_1 & \omega_2 \\ \omega_2 & -\omega_1 & 0 & \omega_3 \\ -\omega_1 & -\omega_2 & -\omega_3 & 0 \end{bmatrix}$$

The gravitational torque is approximated assuming that the distance between the geocenter and the geometric center of the object $\vec{x}$ is much larger than the extension of the object itself for each

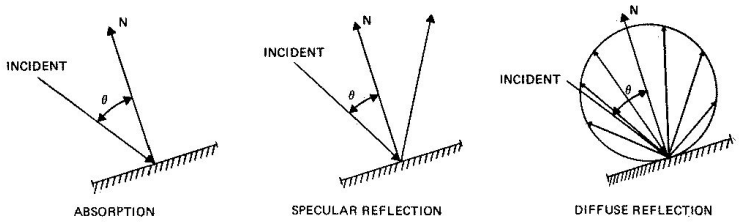

volume element of the object. It can be expressed as the following with the moments of inertia tensor defined in Eq. 2:

$$\vec{\tau}_{\text{grav}} = \frac{GM}{\xi^2}\left[m(\hat{\vec{\xi}} + \vec{\rho}_{\text{grav}}) + \frac{3}{\xi}(\hat{\vec{\xi}} \times (I\hat{\vec{\xi}}))\right] \tag{2}$$

where $\hat{\vec{\xi}} = T \cdot \hat{\vec{x}}$ is the position vector of the object transformed to the body system by the inertial to body transformation matrix T, G is the gravitational constant, M the mass of the Earth, $m = \sum_k m_k$ the total mass of the object, $\vec{\rho}_{\text{grav}}$ is the distance of the geometric center of the object to the center of mass.

2.1. Solar Radiation Pressure

The interaction of light with a surface material may be described in a number of ways. One option is a full bidirectional reflection function (BRDF), the effect of the direct radiation pressure in HAMR object has been investigated [3]. However, a simple approximation is to represent all materials as a mixture of three different processes, specular reflection, Lambertian diffuse reflection and absorption, which are weighted against each other according to material properties with the coefficients C_a, C_s, C_d. If the material is opaque those coefficients add up to one $C_a + C_s + C_d = 1$. The flux on a surface is given by the solar flux, which is equal to the solar constant E at Earth surface, divided by the speed of light c. To find the flux at the object's position it has to be scaled to the appropriate distance. The force acting on a surface is given by the following expression:

$$\vec{F}_{\text{rad}} = \frac{E}{c}\frac{A^2}{|\vec{x} - \vec{x}_{\text{Sun}}|^2} \cdot \vec{f}(A) \tag{3}$$

m is the total mass of the object, A the astronomical unit, $\vec{x}_{\text{Sun}}$ the geocentric position of the sun, c velocity of light, $\vec{S}$ the direction of the radiation source, $\vec{x}$ is the position vector of the object and $\vec{f}(A)$ the area dependent acceleration function.It is sometimes referred to as force function, which is strictly speaking not correct, as this would neglect the mass term.

The reflection function consists of three different parts according to the different kinds of reflection. The absorption exerts the following acceleration on an infinitesimal surface dA:

$$\vec{d}f(A)_{\text{abs}} = -C_a \cos\theta \vec{S} dA, \tag{4}$$

where θ is the angle between the face normal $\vec{N}$ and the sun vector $\vec{S}$. The specular reflection is reflected back in the direction $(-\vec{S} + \vec{N}\cos\theta)$, leading to:

$$\vec{d}f(A)_{\text{spec}} = -C_s(\vec{S} - 2\cos\theta\vec{N} - \cos\theta\vec{S})dA. \tag{5}$$

The diffuse reflection is of a Lambertian surface is distributed proportional to $\cos\phi$, where ϕ is the angle between the reflected radiation and $\vec{N}$. Integrating over all reflection directions leads to:

$$\vec{d}f(A)_{\text{dif}} = -C_d(-\frac{2}{3}\cos\theta\vec{S} - \cos\theta\vec{S})dA. \tag{6}$$

Taking all terms together, analytical solutions can be found for some simple shapes.

For a spherical surface of radius r we get:

$$\vec{f}_{\text{rad,sphere}} = -4\pi\text{r}^2\big(\frac{1}{4} + \frac{1}{9}C_\text{d})\hat{\vec{S}} \tag{7}$$

For a sphere sometimes the parameter C_d is replaced by a single value $\tilde{C} = (\frac{1}{4} + \frac{1}{9}C_\text{d})$. For a flat surface with area A, the acceleration function is:

$$\begin{aligned} \vec{f}_{\text{rad,flat}} &= A\vec{S}\vec{N}\cdot[(1-C_\text{s})\vec{S} + 2(C_\text{s}\cdot\vec{S}\vec{N} + \frac{1}{3}C_\text{d})\vec{N}] \\ \text{for:} &\qquad 0 < \arccos(\hat{\vec{S}}\hat{\vec{N}}_i) < \pi/2 \end{aligned} \tag{8}$$

The absorbed portion of the incident radiation can be re-emitted via thermal radiation. The emission force of a surface A with temperature T is:

$$\vec{F}_{\text{emiss}} = \frac{k}{c}T^4 C_e A\vec{N}, \tag{9}$$

where C_e is the emission coefficient, k is the Stefan Boltzmann constant.

In general the temperature $\tilde{T}$ is approximated via the following (one dimensional) steady state power balance:

$$kAC_{e,f}(\tilde{T}_f^4 - T_{\text{space}}^4) = C_{a,f}A\cdot E\cos\theta\frac{A^2}{|\vec{x}-\vec{x}_{\text{Sun}}|^2} - \sigma A\frac{\tilde{T}_f - \tilde{T}_b}{L} \tag{10}$$

$$kAC_{e,b}(\tilde{T}_b^4 - T_{\text{space}}^4) = \sigma A\frac{\tilde{T}_f - \tilde{T}_b}{L} \tag{11}$$

assuming the solar radiation is incident on the front side of the material. A is the surface/cross sectional area of the material, which appears in all terms of the equation, which is in turn independent of it. $C_{e,f}$ is the front and $C_{e,b}$ back emission coefficient, $\tilde{T}_f$ is the front side and $\tilde{T}_b$ back side temperature, T_{space} the ambient space temperature. $C_{a,f}$ the front side absorption coefficient, σ the thermal conductivity, L the thickness of the material. In order to expand Eq.11 for three dimensions, further coupled equations for the temperatures within the materials have to be added. For thin materials the transmission through the object is often assumed to be immediate, that is the front and the back side temperature would be always the same, as if the thickness would be zero. Setting $\tilde{T}_f = \tilde{T}_b = \tilde{T}$ leads to the following equation for the temperature:

$$\tilde{T} = (C_a\cos\theta E\frac{A^2}{|\vec{x}-\vec{x}_{\text{Sun}}|^2}\frac{1}{k(C_{e,f}+C_{e,b})} + T_{\text{space}}^4)^{\frac{1}{4}} \tag{12}$$

In general, a further simplification is made such that the space ambient temperature is assumed to be exactly zero Kelvin. Hence, most commonly the temperature $\tilde{T}$ is approximated via the following steady state power balance [14]:

$$A \cdot C_a \cdot \cos\theta E \frac{A^2}{|\vec{x}-\vec{x}_{\text{Sun}}|^2} = k\tilde{T}^4 (C_{e,f} + C_{e,b}) \cdot A \tag{13}$$

Again, this is neglecting any surface thermal transport and a direct thermal transport throughout the object and a zero ambient temperature. This leads to the following equation for the temperature:

$$\tilde{T} = (C_{a,f} \cos\theta E \frac{A^2}{|\vec{x}-\vec{x}_{\text{Sun}}|^2} \frac{1}{k(C_{e,f}+C_{e,b})})^{\frac{1}{4}} \tag{14}$$

This leads to the following emission force expression:

$$\tilde{\vec{F}}_{\text{emiss}} = A\frac{E}{c} C_{a,f} \cos\theta \frac{A^2}{|\vec{x}-\vec{x}_{\text{Sun}}|^2} \cdot \frac{C_{e,f}}{(C_{e,f}+C_{e,b})} \vec{N}, \tag{15}$$

The emission force is the equal to the absorption force (Eq.3 and 4) redirected in the direction of the normal vector and scaled by the emission coefficients of the front and back side in this model. For identical emission coefficients, the absolute value of the absorption force is scaled by 0.5. The steady state power balance has often been used [10, 6, 7]. It has the advantage that it even allows to combine the front side and back side equations into one temperature expression, such that the thermal emission of both sides can be calculated in one step only. However, it has several shortcomings. Because of the steady state assumption, the model does not take the thickness of the material into account, and the transmission through the object is seen as immediate. The temperature drops immediately to zero, as soon as the incoming radiation ceases. This would be also true if parts of the object would be self-shadowed, which means that in our calculation one part of the object could in case of self-shadowing immediately have zero temperature and adjacent sun-light parts have a high temperature. Multi-layer insulation materials, however, are build to isolate, and hence, an immediate heat transfer is probably not an accurate description. More fundamentally, if we add the front side $\tilde{\vec{F}}_{\text{emiss,f}}$ and back side force $\tilde{\vec{F}}_{\text{emiss,b}}$on a plate like object together, the net force is directly proportional to the difference in the emission coefficient.

$$\begin{aligned} \tilde{\vec{F}}_{\text{emiss,f}} + \tilde{\vec{F}}_{\text{emiss,b}} &\propto C_{e,f}\vec{N}_f + C_{e,b}\vec{N}_b \\ \text{if } \vec{N}_f = -\vec{N}_b \text{ and } C_{e,f} = C_{e,b} &\longrightarrow \tilde{\vec{F}}_{\text{emiss,f}} + \tilde{\vec{F}}_{\text{emiss,b}} = \vec{0} \end{aligned} \tag{16}$$

For any object with identical front side and back side material, and hence emission coefficients, the thermal radiation is always zero, as half the incoming energy is equally radiated outwards on the back and and the front, and hence is identically to a model neglecting this effect. There have been attempts to enhance the model deficiencies with empirical models or at least the introduction of so-called lag parameters [15].

Another way is to focus on the physical process of heat transfer instead of the steady state solution and find a computationally efficient way to solve the heat transfer equation, which in the

current case has the following form:

$$\frac{\partial T}{\partial t} - \alpha \Delta T = \frac{1}{c_p \rho}\Big(kC_e \nabla (T_{\text{space}}^4 - T^4) + \nabla G_{\text{gen}}\Big), \tag{17}$$

$$G_{\text{gen}} = C_a \cos\theta E \frac{A^2}{|\vec{x} - \vec{x}_{\text{Sun}}|^2} \tag{18}$$

T is the temperature, $\alpha = \frac{\sigma}{c_p \rho}$ is the thermal diffusivity, where σ is the thermal conductivity, c_p is the specific heat capacity, and ρ is the density of the material, G_{gen} is the heat generated on the surface of the object by the incoming radiation. Note that the derivatives are taken over the object itself in the object coordinate frame. The steady state equations can be derived from the transient ones in setting the time derivative to zero.

A straight forward solution of the above heat transfer equation would be to use numerically integrated finite element methods. The disadvantage is that a full finite element solution is computationally expensive, especially when combined in a simultaneous six degree of freedom orbit integration. We choose the alternative to approximate the partial differential equation via finite differences. Finite differences can be understood as the solution of the weak form of the PDE where the integrals are solved via trapezium rule under the assumption of equidistant elements under utilization of Garlekin method[16]. This leads to the following equation using the Taylor series expansion to derive the finite differences to replace the derivatives of first and second order. In the equation below, we assume a boundary on the surface in z-direction:

$$\begin{aligned}
&\frac{\partial T_i}{\partial t} - \alpha\Big(\frac{T_i(x_i + l, y_i, z_i) - 2T_i(x_i, y_i, z_i) + T_i(x_i - l, y_i, z_i)}{\Delta x_{\text{body}}^2} \\
&+ \frac{T_i(x_i, y_i + l, z_i) - 2T_i(x_i, y, z) + T_i(x_i, y_i - l, z_i)}{\Delta y_{\text{body}}^2} \\
&+ \frac{T_i(x_i, y_i, z_i - d) - T_i(x_i, y_i, z_i)}{\Delta z_{\text{body}}^2}\Big) = \\
&\frac{1}{c_p \rho \Delta z_{\text{body}}}\Big(C_e k (T_{\text{space}}^4 - T_i^4(x_i, y_i, z_i)) + C_a \cos\theta E \frac{A^2}{|\vec{x} - \vec{x}_{\text{Sun}}|^2}\Big),
\end{aligned} \tag{19}$$

where the temperatures are defined for each sub-volume element i. The x_{body} and y_{body} direction are on the surface of the object. The z direction is in direction through the object, z_{body}, Δ denotes the difference between two reference points in the finite differences. The temperature of each subelement at the next time step t+1 is then calculated using finite differences:

$$T_{i,t+1} = T_{i,t} + \frac{dT_i}{dt} \cdot \Delta t \tag{20}$$

This leads to the possibility having different temperatures on both sides of the materials as well as taking self-shadowing effects into account where differences in the temperature of adjacent parts of the objects are influencing each other. That means, thermal effects take place, even when the emission coefficient of both sides is identical. This also means, temperature gradients over the object is possible. However, this reduces the computational burden tremendously, but allowing

Table 1: Fabrication values of MLI pieces[17]: coating, AMR value $[m^2/kg]$, reflection (specular and diffuse) absorption and emission values (C_s, C_d, C_a), thermal conductivity σ ([W/mk], specific heat c_p [J/kgK] and the density ρ [kg/m^3][17, 18].

Kapton [37.5μm]	AMR	C_s	C_d	C_a	C_e	σ	c_p	ρ
alum coated.	26.3	0.60	0.26	0.14	0.26	0.12	$1.09{\cdot}10^3$	$1.52{\cdot}10^3$

for an improved temperature model and thermal radiation pressure modeling nevertheless. What remains are stability limitations, for the temperature transmission through this very thin material, which requires small times steps. The stability condition is:

$$\frac{\alpha \Delta t}{\Delta x} \leq \frac{1}{2} \tag{21}$$

3. Simulation

The multi-layer material Kapton [17] has been simulated. The material properties are listed in Table 1. The thickness of the object is 37.5μm, the object is tessellated in nine-surface resp. volume elements. For the thermal conductivity a constant value was assumed although it is well established that those values vary with temperature. But as the variations are small within the temperature band compared to the absolute values, this was not taken into account. A reference value of around 90 Kelvin was chosen. The coating is so thin, that the surface properties are adapted and the volumetric thermal properties are the same as the uncoated object.

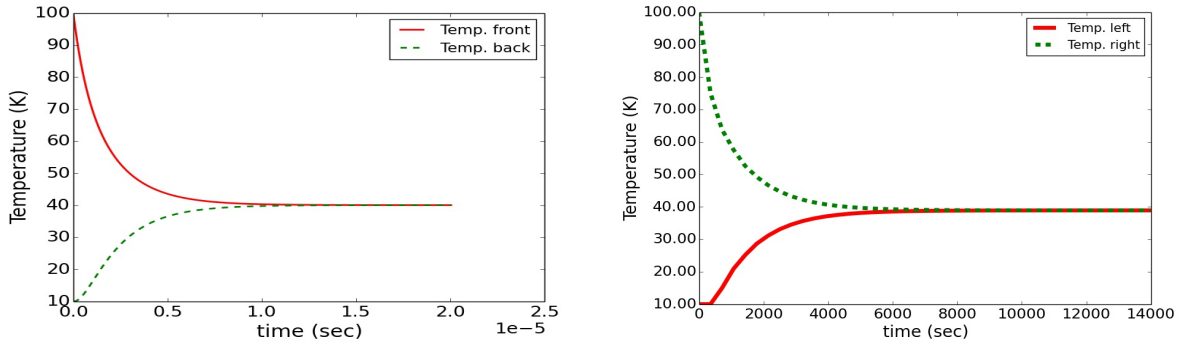

(a) (b)

Figure 1: **Transient thermal evolution of a perfectly isolated fully coated piece of MLI.**

A flat object geometries has been used, which has been investigated in the absence of thermal re-radiation [3, 5]. The object is assumed to be a rigid body, which is, given the properties of MLI, maybe not a very good approximation. The object is assumed to be coated with aluminum on both sides, hence having the same emission coefficient on either side. The object is first simulated neglecting thermal re-radiation completely, secondly using the oversimplified steady state model, as in Eq. 13 to 15 is explained, and thirdly, by using the transient model in Eq.18 and 19. At

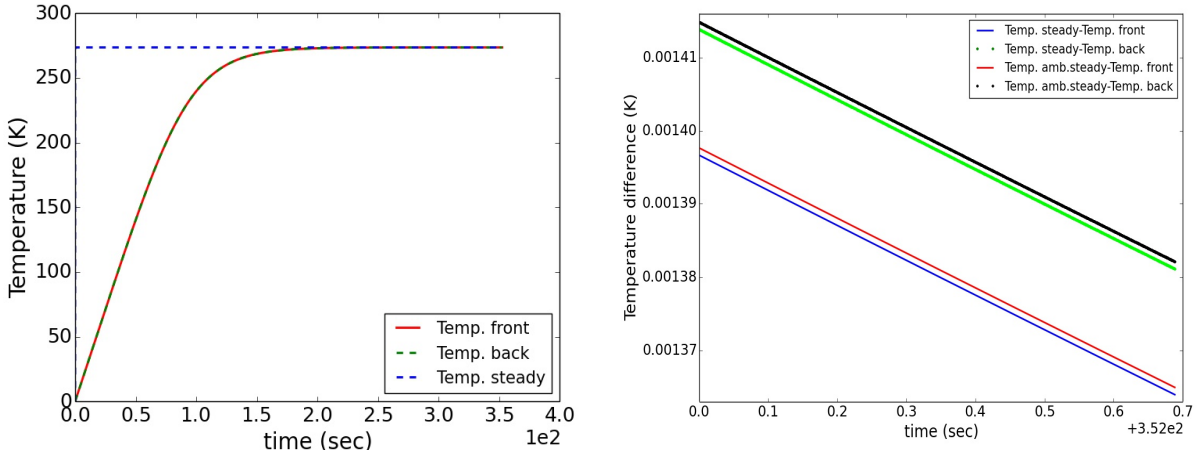

(a) (b)

Figure 2: **a) Steady state (with 0K, and with 3K ambient temperature) and transient temperature with incoming radiation at one AU for a both side coated Kapton object, b) differences between steady state and transient temperatures on both sides.**

first we investigate the thermal properties of the object. In Fig.1a) the object isolated object has a temperature of 100K at the front side and 10K at the back side. Without ambient temperature exchange nor incoming radiation the temperature on the back and front side quickly equal each other. As a comparison, the steady state power law derived temperature for this example would be zero, as there is no incoming radiation. Fig.1b) shows the temperature evolution if the temperature is 100K on one end left end of the object (back and front identical) and 10K on the right end of the object (back and front identical) with side length of one meter. It takes 6000 seconds, more than 1.5 hours, till a steady temperature is reached.

In a next step, the ambient temperature of three Kelvin and the incoming radiation at a one AU distance to the sun is added. The object is kept at a constant orientation of 90 degrees of the object surface to the sun orientation. Fig.2a) shows the heating of the object from zero degrees Kelvin calculated with the transient model, and the steady state model. It shows that after 250 to 300 seconds (around 5 minutes) the object is heated to a comparable temperature to the steady state one. Fig.2b) shows the temperature differences between the transient and steady state temperatures of the front resp. back side of the object, revealing that even after 353 seconds the simplified steady state temperature is not reached. A temperature difference between the front side and back side persists. Using the ambient temperature of 3K does not introduce a significant change.

Fig.3a) shows that the temperature difference is constant over time as the object heats up. It is governed by the thickness and the conductivity of the object. It is also intuitively obvious that the front side that is subject to the direct radiation keeps to be a bit warmer than the back side, see also Eq.11. Because the emission force depends on the temperature differences each in the power of four Eq.9, it increases as the object heats up. The comparison in Fig.3c) shows that the thermal emission force is still orders of magnitudes smaller than the direct radiation pressure. Still, it has to be noted that for the steady state model in the case where the emission coefficient on the front

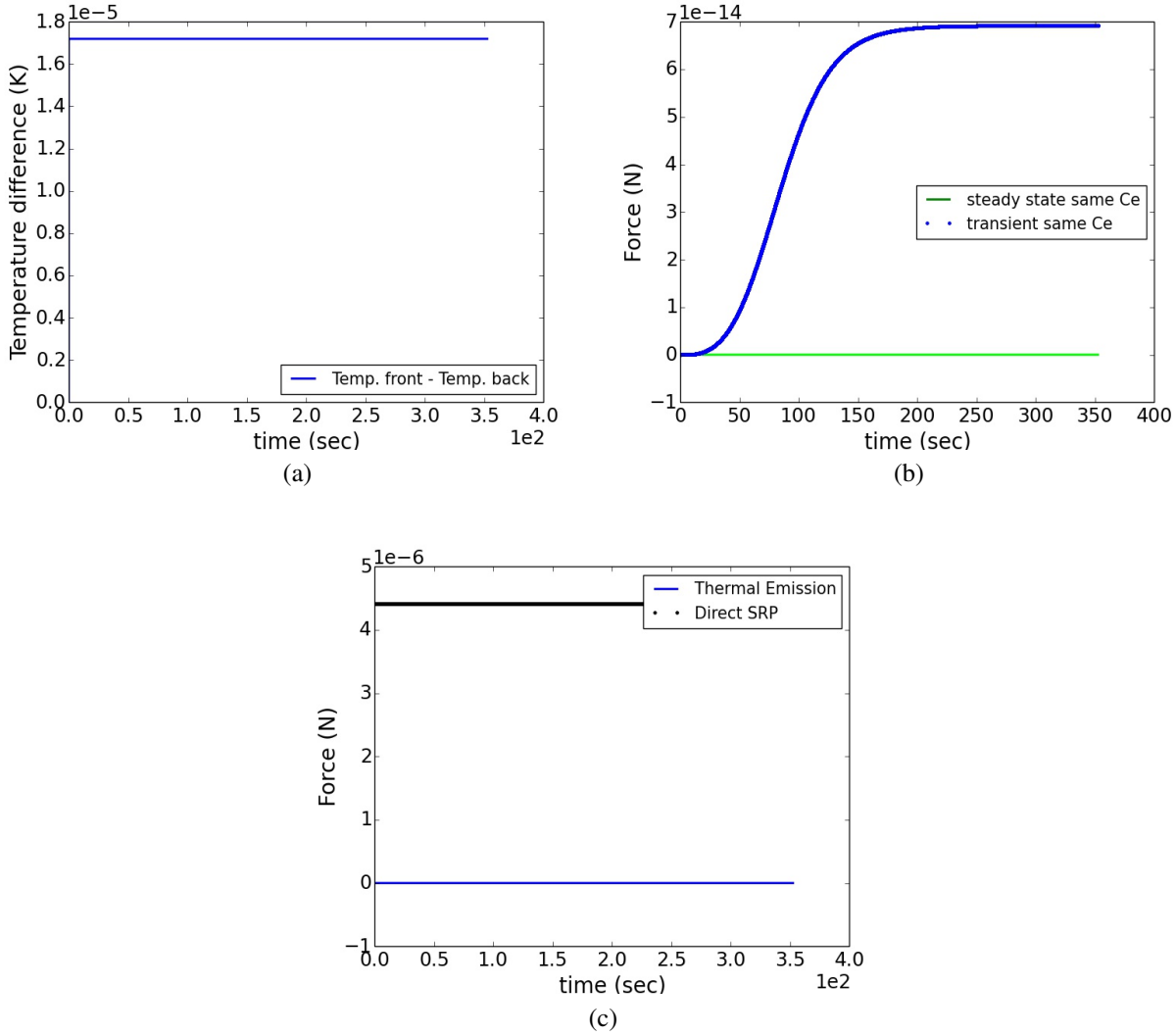

Figure 3: **a) Temperature difference of the front side to the back side as a function of time in the heating process from 0K for the transient model, b) Emission forces from the transient and steady state model for the same emission coefficient on the front and back side. c) Comparison between the direct radiation pressure forces and the thermal radiation force for the transient model.**

and back side is the same, this value is exactly zero. Furthermore, the thermal re-radiation is only surface dependent and not dependent on the sun direction.

4. Conclusions

A flat high-area-to-mass ratio object has been simulated.The radiation forces acting on the object have been evaluated. In particular the thermal force models, the simplified steady state and the transient model have been compared. It takes considerable time for an object to heat up from zero Kelvin, furthermore the transient state model reveals that there is a constant temperature difference

maintained, as the sun lit side is always a bit warmer than the side facing away from the sun. This means in contrast to the steady state model, thermal forces are not zero when the object has the same emission parameters on both sides. It has to be kept in mind that the thermal forces are an order of magnitude smaller than direct radiation pressure forces. Further investigations have to be performed to evaluated the effects on the orbit of a space object.

5. Acknowledgments

I would like to acknowledge the work of Sergio Rodriguez, who looked into some of the empirical thermal models during his master thesis.The work has been supported by the Los Alamos National Laboratory in the realm of the IMPACT project.

6. References

[1] Schildknecht, T., Musci, R., Ploner, M., Beutler, G., Kuusela, J., de León Cruz, J., and de Fatima Domínguez Palmero, L. "Optical Observations of Space Debris in GEO and in Highly-Eccentric Orbits." Advances in Space Research, Vol. 34, No. 5, pp. 901–911, 2004.

[2] Schildknecht, T., Musci, R., Ploner, M., Hugentobler, U., Serra Ricart, M., de León Cruz, J., and de Fatima Domínguez Palmero, L. "Geostationary Orbit Objects Survey." Final Report, ESA ESOC Contract 11914/96/D/IM, 2004.

[3] Früh, C., Kelecy, T., and Jah, M. "Coupled Orbit-Attitude Dynamics of High Area-to-Mass Ratio (HAMR) Objects: Influence of Solar Radiation Pressure, Earth's Shadow and the Visibility in Light Curves." Celestial Mechanics and Dynamical Astronomy, Vol. 117, pp. 385–404, 2013.

[4] Frueh, C. and Jah, M. "Attitude and Orbit Propagation of High Area-to-Mass Ratio (HAMR) Objects using a Semi-Coupled Approach." Journal of Astronautical Science, Vol. DOI 10.1007/s40295-014-0013-1, July 2014.

[5] Früh, C. and Jah, M. "Coupled Orbit-Attitude Motion of High Area-to-Mass Ratio (HAMR) Objects Including Efficient Self-Shadowing." Acta Astronautica, Vol. 95, pp. 227–241, 2014.

[6] McMahon, J. and D.J.Scheeres. "A New Navigation Force Model for Solar Radiation Pressure." Journal of Guidance, Control, and Dynamics, Vol. 33, No. 5, pp. 1418–1428, 2010.

[7] McMahon, J. and D.J.Scheeres. "Appropriate Modeling of Solar Radiation Pressure Effects on Uncontrolled Orbiting Objects for Accurate Dynamical Predictions." "AAS/AIAA Space Flight Mechanics Meeting, Charleston, SC," 2012.

[8] Öpik, E. and Lindsay, E. "Collision probabilities with the planets and the distribution of interplanetary matter." "Proceedings of the Royal Society of London., Series A, Mathematical and physical sciences," Vol. 54, A, no. 12.2. 1951.

[9] Paddack, S. and Rhee, J. "Rotational bursting of interplanetary dust particles." Geophysical Research Letters, Vol. 2, No. 365, 1975.

[10] Albuja, A., Scheeres, D., and McMahon, J. "Evolution of Anglar Velocity for Space Debris as a Result of YORP." "Proceedings of the Space Flight Mechanics Meeting, Kauai, HI," 2013.

[11] Frueh, C. "Effects of Thermal Re-radiation on Orbit and Attitude of High Area-to-Mass Ratio Objects Using Different Models: YORP and YASKOWSKI." 21th AAS/AIAA Space Flight Mechanics Meeting, Williamsburg, VA, January 2015. 15-403.

[12] Pines, S. "Uniform Representation of the Gravitational Potential and its Derivatives." AIAA Journa, Vol. 11, No. 11, pp. 1508–1511, 1973.

[13] Wertz, J. Spacecraft Attitude Determination and Control. Volume 73. D.Reidel Publishing Company, Dordrecht: Holland, 1978. ISBN: 90-277-0959-9.

[14] McInnes, C. Solar Sailing: Technology, Dynamics and Mission Applications. Springer-Praxis, Chichester, UK, 1999. ISBN-13: 978-3540210627.

[15] Kelecy, T. and Jah, M. "Analysis of Orbit Prediction Sensitivity to Thermal Emissions Acceleration Modeling for High Area-to-mass Ratio Objects." "Advanced Maui Optical and Space Surveillance Technologies Conference," 2009.

[16] Yip (ed.), S., Peiró, J., and Sherwin., S. Handbook of Materials Modeling. Volume I: Methods and Models, chapter 8.2, 2415-2446. Springer, Netherlands, 2005. ISBN 978-1-4020-3286-8.

[17] Sheldahl. "The Red Book." /http://www. sheldahl.com/product/bulletins/RedBook.pdf, 2009.

[18] Benford, D., Powers, T., and Moseley, S. "Thermal conductivity of Kapton tape." Cryogenics, Vol. 39, No. 1, pp. 93 – 95, 1999. ISSN 0011-2275.